Hindawi
Structural Control and Health Monitoring
Volume 2023, Article ID 6658364, 16 pages
https://doi.org/10.1155/2023/6658364

WILEY | Hindawi

Research Article

Real-Time Integration of Identification and Semiactive Optimization Control for Mass Damper-Building Combined Systems under Known/Unknown Seismic Excitations

Chang Yin,[1] **Jubin Lu**,[2] **Chunyan Xiang**,[1] **and Ying Lei**[1,3]

[1]*Department of Civil Engineering, Xiamen University, Xiamen 361005, China*
[2]*Department of Civil and Environmental Engineering, The Hong Kong Polytechnic University, Hung Hom, Hong Kong, China*
[3]*Xiamen Key Laboratory of Integrated Application of Intelligent Technology for Architectural Heritage Protection, Xiamen University, Xiamen, China*

Correspondence should be addressed to Ying Lei; ylei@xmu.edu.cn

Received 30 June 2023; Revised 27 October 2023; Accepted 29 November 2023; Published 15 December 2023

Academic Editor: Chao Sun

The integration of structural identification and vibration optimal control has been studied. Since the semiactive optimization vibrational control of civil structures needs to be implemented by massive control devices such as mass dampers, it is necessary to investigate the real-time integration of identification and semiactive optimization vibration control for mass damper-building combined systems. However, there is a lack of such studies in the literature. In this paper, a methodology is presented for real-time integration of identification and semiactive optimization vibration control of the mass damper-building combined system under known/unknown seismic excitations. For the combined system under known seismic excitations, the identification is implemented by the extended Kalman filter (EKF) using only partial structural acceleration responses. The identified structural state and parameters of mass damper-building systems are integrated in real time for the optimal control of systems by the linear-quadratic regulator (LQR) control algorithm and the Hrovat semiactive optimization control strategy via semiactive optimization mass dampers (SAMD). Then, it is extended to the scenario of unknown seismic excitations. The partially measured structural acceleration responses are absolute ones in this case, so the generalized extended Kalman filter with unknown input (GEKF-UI) developed by the authors is used to identify the structural input-state parameters of the mass dampers-building combined systems. The identification results are also integrated in real time for the semiactive optimization control of the combined system via SAMD. Two numerical simulation examples are used to test the proposed integration methods. It is shown that the proposed integration methods can reach almost the same optimal control effects as the conventional semiactive optimization control with known parameters of the mass damper-building combined systems under known/unknown seismic excitations.

1. Introduction

Severe external excitations such as seismic actions or wind loads produce adverse vibration responses to structures, so health monitoring and vibration control of structures under such severe excitations have been widely concerned [1–4]. In order to realize structural optimal vibration control, structure state and parameters need to be identified. At the same time, structural health monitoring (SHM) systems and vibration control systems are also two important components for smart structures [5, 6]. Therefore, it is essential to integrate structural health monitoring and structural vibration control techniques for structural safety, reliability, and intelligence.

In the past decades, some studies have been conducted on the integration of SHM and vibration control. Gattulli and Romeo [7] proposed an adaptive active control approach for MDOF linear structures by combining the sliding mode control with errors tracking-based damage detection; Sun and Tong [8] identified the debonding of piezoelectric actuator patches in controlled structures based on the frequency shift. Yang et al. [9] experimentally studied the

integration method by using a controlled 3-story aluminum frame, where stiffness reduction was used to model the structural damage. The authors [10] also proposed an extended Kalman filter (EKF)-based algorithm for detecting abrupt damage, and the updated model was then online integrated with the structural active control algorithm. The above studies mainly focused on integrating system identification with structural active control schemes, which require large external energy inputs. Chen et al. [11] and Huang et al. [12] studied the integration of structural system identification and semiactive optimization control by semiactive optimization friction dampers in time and frequency domains, respectively. However, the most studies mentioned above require a lot of knowledge of structural parameters and external excitations.

In practical applications, it may be hard to precisely measure external excitations. Therefore, there are methodologies for the integrated structural system identification and vibration control under unknown excitation. He et al. [13, 14] investigated the synthesis, identification, and vibration control of structures with unknown inputs. Xu et al. [5] also explored the integration of health monitoring and vibration control for smart building structures with time-varying structural parameters and unknown excitation. The authors [15] proposed a general synthesis of identification and vibration control of building structures under unknown excitations and presented the integration of identification and vibration control of time-varying structures subject to unknown seismic excitations [16].

Especially, structural semiactive optimization control has energy efficiency, multimode control, active adaptability, impact resistance, adjustability, and flexibility in the structural vibration control [3, 17, 18]. Therefore, the investigation of integrated structural health monitoring and semiactive optimization control of structures has attracted many scholars, e.g., Xu and Chen [19, 20] proposed the integrated system of vibration control and health monitoring based on semiactive friction dampers to achieve model updating, seismic response control, and damage detection of building structures. Simon and Okyay [21] investigated a vibration control algorithm with variable stiffness-tuned mass dampers combined with a nonlinear system identification method for the control of multistory shear frame structures which exhibit abrupt stiffness degradations. Since the semiactive optimization control of civil structures needs to be implemented by massive control devices such as mass dampers, it is necessary to investigate the real-time integration of identification and semiactive optimization control for mass damper-building combined systems. However, there is a lack of such study, in the literature. Chang et al. [22] presented an algorithm for parameter identification of active mass damper (AMD) or tuned mass damper (TMD)-building coupled systems using acceleration measurements, but full measurements of structural acceleration responses are required [23]. Kang et al. [24] evaluated the dynamic performance of the TMD under a typhoon using system identification. The TMD-structure system is assumed to be a two degrees of freedom model, and the natural frequency of the TMD and structure is estimated according to the frequencies of the coupled system without considering damping.

This paper aims at presenting a method of real-time integration of identification and semiactive optimization control for mass damper-building combined systems under known/unknown excitations. First, the integrated identification of mass damper-building combined systems and semiactive optimization control under known seismic excitation is studied. The identification of mass damper-building combined systems is implemented by the extended Kalman filter (EKF) using partial structural acceleration responses, and the identification results are integrated in real time with the optimal semiactive optimization control of structural systems. Then, it is extended to investigate the integrated identification of mass damper-building combined systems and semiactive optimization control under unknown seismic excitation. In this case, the generalized extended Kalman filter with unknown input (GEKF-UI), recently proposed by the authors, is used to identify the input-state parameters of the mass damper-structure combined systems and integrated in real time with the optimal semiactive optimization vibration control of structures by semiactive optimization mass damper (SAMD). Numerical simulation examples are used to test the proposed methods.

The rest of this paper is organized as follows: Section 2 first presents the identification methods for semiactive optimization mass damper-building combined systems under known/unknown excitation, respectively, and then shows the real-time integration with structural semiactive optimization vibration control. Section 3 validates the proposed methods through numerical simulation work with a multistory shear frame under seismic excitations. Finally, Section 4 discusses the research conclusions.

2. The Proposed Methodology

This paper aims at providing methodology for the integrated identification of mass damper-building combined systems and vibration control under known/unknown seismic excitations. As shown in Figure 1, a semiactive mass damper (SAMD) is installed in a n-story building structure to reduce its vibration response under seismic excitation $\ddot{x}_g(t)$.

The equation of motion of the mass damper-building combined system under seismic excitation can be expressed as follows:

$$\mathbf{M}\ddot{\mathbf{x}}(t) + \mathbf{C}\dot{\mathbf{x}}(t) + \mathbf{K}\mathbf{x}(t) = -\mathbf{M}\mathbf{I}_g\ddot{x}_g(t) + \boldsymbol{\eta}^c u(t), \quad (1)$$

where $\mathbf{x}$ is the displacement vector relative to the ground motion, $\mathbf{x} = [x_1\, x_2 \cdots x_n\, x_s]^T$, x_i and x_s are the displacement of the i-th floor building and the SAMD relative to the ground, respectively, $\mathbf{M}$, $\mathbf{C}$, and $\mathbf{K}$ are the mass, damping, and stiffness matrices of the damper-building combined system, respectively, $\mathbf{I}_g$ is the influence vector of the seismic excitation $\ddot{x}_g(t)$, and u(t) is the control force of the SAMD with location vector $\boldsymbol{\eta}^c$.

For a mass damper-shear building combined system,

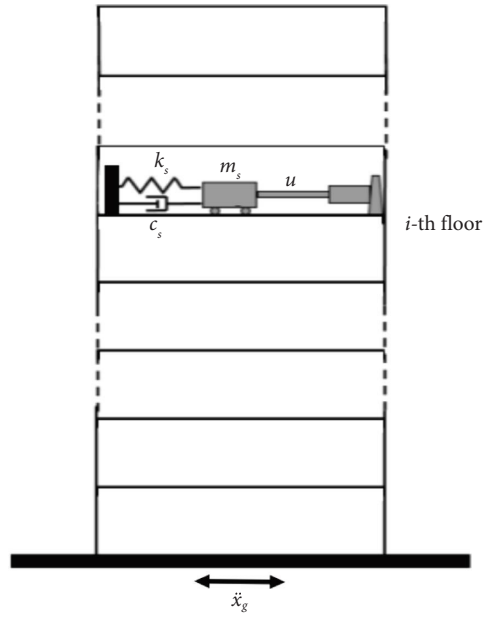

Figure 1: A SAMD-building combined system under seismic excitations.

$$\mathbf{M} = \begin{bmatrix} \mathbf{m} & \mathbf{m}_a^T \\ \mathbf{m}_a & m_s \end{bmatrix}; \mathbf{C} = \begin{bmatrix} \mathbf{c} & \mathbf{c}_a^T \\ \mathbf{c}_a & c_s \end{bmatrix}; \mathbf{K} = \begin{bmatrix} \mathbf{k} & \mathbf{k}_a^T \\ \mathbf{k}_a & k_s \end{bmatrix}, \tag{2}$$

in which, $\mathbf{m}$, $\mathbf{c}$, and $\mathbf{k}$ are the mass, damping, and stiffness matrices of the building structure, respectively, m_s, c_s, and k_s are the mass, damping, and stiffness parameters of the SAMD, respectively; $\mathbf{m}_a$, $\mathbf{c}_a$, and $\mathbf{k}_a$ are the mass, damping, and stiffness matrix of the main structure coupled with the SAMD, respectively,

$$\mathbf{m}_a = [0\ 0 \cdots 0]_{1\times n}; \mathbf{c}_a = [0\ 0 \cdots -c_s \cdots 0]_{1\times n}; \mathbf{k}_a = [0\ 0 \cdots -k_s \cdots 0]_{1\times n}. \tag{3}$$

2.1. Identification of SAMD-Building Combined Systems under Known Seismic Excitations. For the SAMD-building combined structural system under known seismic excitation, the extended Kalman filter (EKF) can be used to identify the structural state and parameters of the combined system using partial measurements of acceleration responses relative to the ground motion $\ddot{x}_g$.

The extended state vector of the SAMD-building combined system is expressed as $\mathbf{Z} = [\mathbf{x}\,\dot{\mathbf{x}}\,\theta]^T$, where $\boldsymbol{\theta}$ denotes the vector of the unknown parameters, including the damping and stiffness parameters of the main structure and the SAMD. Then, equation (1) can be expressed in the state equation as follows:

$$\begin{aligned} \dot{\mathbf{Z}} &= \begin{Bmatrix} \dot{\mathbf{x}} \\ \ddot{\mathbf{x}} \\ \dot{\boldsymbol{\theta}} \end{Bmatrix} = \begin{Bmatrix} \dot{\mathbf{x}} \\ \mathbf{M}^{-1}\left(-\mathbf{M}\mathbf{I}_g\ddot{x}_g + \boldsymbol{\eta}^c u - \mathbf{C}\dot{\mathbf{x}} - \mathbf{K}\mathbf{x}\right) \\ \mathbf{0} \end{Bmatrix} \\ &= \begin{Bmatrix} \dot{\mathbf{x}} \\ -\mathbf{M}^{-1}(\mathbf{C}\dot{\mathbf{x}} + \mathbf{K}\mathbf{x}) \\ \mathbf{0} \end{Bmatrix} + \begin{Bmatrix} \mathbf{0} \\ -\mathbf{I}_g \\ \mathbf{0} \end{Bmatrix}\ddot{x}_g + \begin{Bmatrix} \mathbf{0} \\ \mathbf{M}^{-1}\boldsymbol{\eta}^c \\ \mathbf{0} \end{Bmatrix} u \\ &= \mathbf{g}(\mathbf{Z}) + \mathbf{B}\ddot{x}_g + \mathbf{B}^c u. \end{aligned} \tag{4}$$

Since the ground acceleration $\ddot{x}_g(t)$ is known, some structural relative acceleration responses can be measured so that the observation equation can be expressed as:

$$\begin{aligned}\mathbf{y} = \mathbf{L}_a\ddot{\mathbf{x}} &= \mathbf{L}_a\mathbf{M}^{-1}\left[(-\mathbf{C}\dot{\mathbf{x}} - \mathbf{K}\mathbf{x}) + \mathbf{I}_g\ddot{x}_g + \boldsymbol{\eta}^c u\right] \\ &= \mathbf{h}(\mathbf{Z}) + \mathbf{D}\ddot{x}_g + \mathbf{D}^c u,\end{aligned} \tag{5}$$

where $\mathbf{y}$ is the observation vector and $\mathbf{L}_a$ denotes the accelerometer location matrix.

Based on the state equation of equation (4) and the observation equation of equation (5), the extended Kalman filter (EKF) method is used to identify the damper-building combined system.

First, the prediction of the extended state vector is derived based on equation (4) as follows:

$$\widetilde{\mathbf{Z}}_{k+1|k} = \widehat{\mathbf{Z}}_{k|k} + \int_{k\Delta t}^{(k+1)\Delta t}\left[\mathbf{g}\left(\widehat{\mathbf{Z}}_{t|k}\right) + \mathbf{B}\ddot{x}_{g,t|k} + \mathbf{B}^c\widehat{u}_{t|k}\right]\mathrm{d}t, \tag{6}$$

and the predicted error matrix is given by

$$\widetilde{\mathbf{P}}_{k+1|k} = \boldsymbol{\Phi}_{t|k}\widehat{\mathbf{P}}_{t|k}\boldsymbol{\Phi}_{t|k}^T + \mathbf{Q}_k, \tag{7}$$

in which, $\boldsymbol{\Phi}_{t|k} \approx \mathbf{I} + \Delta t\mathbf{G}_{t|k}$ and $\mathbf{I}$ is the identity matrix, $\mathbf{G}_{t|k} = \partial g(\mathbf{Z})/\partial\mathbf{Z}|\mathbf{Z} = \widehat{\mathbf{Z}}_{t|k}$, and $\mathbf{Q}_k$ is the state error covariance matrix.

Then, the extended state vector is corrected/estimated using the observation equation of equation (5) as follows:

$$\widehat{\mathbf{Z}}_{k+1|k+1} = \widetilde{\mathbf{Z}}_{k+1|k} + \mathbf{K}_{k+1}\left[\mathbf{y}_{k+1} - \mathbf{h}\left(\widetilde{\mathbf{Z}}_{k+1|k}\right) - \mathbf{D}\ddot{x}_{g,k+1} - \mathbf{D}^c\widehat{u}_{t|k}\right], \tag{8}$$

and $\mathbf{K}_{k+1}$ denotes the Kalman gain matrix, which can be expressed as follows:

$$\mathbf{K}_{k+1} = \widetilde{\mathbf{P}}_{k+1|k}\mathbf{H}_{k+1|k}^T\left(\mathbf{H}_{k+1|k}\widetilde{\mathbf{P}}_{k+1|k}\mathbf{H}_{k+1|k}^T + \mathbf{R}_{k+1}\right)^{-1}, \tag{9}$$

in which, $\mathbf{H}_{k+1|k} = \partial\mathbf{h}(\mathbf{Z})/\partial\mathbf{Z}|\mathbf{Z} = \widetilde{\mathbf{Z}}_{k+1|k}$ and $\mathbf{R}_{k+1}$ is the observation noise covariance matrix.

The estimated error matrix is given by

$$\begin{aligned}\widehat{\mathbf{P}}_{k+1|k+1} = &\left(\mathbf{I} - \mathbf{K}_{k+1}\mathbf{H}_{k+1|k}\right)\widetilde{\mathbf{P}}_{k+1|k}\left(\mathbf{I} - \mathbf{K}_{k+1}\mathbf{H}_{k+1|k}\right)^T \\ &+ \mathbf{K}_{k+1}\mathbf{R}_{k+1}\mathbf{K}_{k+1}^T.\end{aligned} \tag{10}$$

2.2. Identification of SAMD-Building Combined Systems under Unknown Seismic Excitation. In this case, the seismic ground acceleration $\ddot{x}_g(t)$ is unknown. The relative acceleration response of the building structure cannot be measured, and the observation equation is for structural absolute acceleration responses. Therefore, there is no direct feedback of the unknown input $\ddot{x}_g(t)$ in the observation equation, and the generalized Kalman filter with unknown input (GEKF-UI), which was recently proposed by the authors [15, 16, 25], is adopted herein for the identification. Moreover, some measurements of structural interstory displacements are also used to avoid the "drift" problem in the identification results [16, 25]. Therefore, the observation equation is written as follows:

$$\begin{aligned}\mathbf{y} &= \begin{Bmatrix}\mathbf{L}_a\ddot{\mathbf{x}}_a \\ \mathbf{L}_d\mathbf{d}\end{Bmatrix} \\ &= \begin{Bmatrix}-\mathbf{L}_a\mathbf{M}^{-1}(\mathbf{C}\dot{\mathbf{x}} + \mathbf{K}\mathbf{x}) \\ \mathbf{L}_d\mathbf{T}\mathbf{x}\end{Bmatrix} + \begin{Bmatrix}\mathbf{L}_a\mathbf{M}^{-1}\boldsymbol{\eta}^c \\ \mathbf{0}\end{Bmatrix}u = \mathbf{h}(\mathbf{Z}) + \mathbf{D}^c u,\end{aligned} \tag{11}$$

where $\ddot{\mathbf{x}}_a = \ddot{\mathbf{x}} + \ddot{x}_g$ is the absolute acceleration response vector while $\mathbf{d}$ denotes the interstory displacement vector; $\mathbf{L}_a$ and $\mathbf{L}_d$ are the corresponding sensor location matrices; and $\mathbf{T}$ represents the conversion matrix between the interstory displacement and relative displacement.

First, $\mathbf{g}(\mathbf{Z}_k)$ in equation (4) can be linearized at $\mathbf{Z}_k = \widehat{\mathbf{Z}}_{k|k}$ by the Taylor series expansion to the first order as follows:

$$\mathbf{g}(\mathbf{Z}_k) = \mathbf{g}\left(\widehat{\mathbf{Z}}_{k|k}\right) + \mathbf{G}_{k|k}\left(\mathbf{Z}_k - \widehat{\mathbf{Z}}_{k|k}\right), \tag{12}$$

in which, $\widehat{\mathbf{Z}}_{k|k}$ denotes the estimated $\mathbf{Z}_k$ with the measurements $(\mathbf{y}_1, \mathbf{y}_2, \ldots, \mathbf{y}_k)$; $\mathbf{G}_{k|k} = \partial\mathbf{g}(\mathbf{Z})/\partial\mathbf{Z}|\mathbf{Z} = \widehat{\mathbf{Z}}_{k|k}$.

Similarly, the observation equation equation (11) is linearized as follows:

$$\mathbf{y}_{k+1} = \mathbf{H}_{k+1|k}\mathbf{Z}_{k+1} + \mathbf{D}^c u_{k+1} + \mathbf{h}_{k+1|k} + \nu_{k+1}, \tag{13}$$

in which $\mathbf{H}_{k+1|k} = \partial\mathbf{h}(\mathbf{Z}_{k+1})/\partial\mathbf{Z}_{k+1}|\mathbf{Z}_{k+1} = \overline{\mathbf{Z}}_{k+1|k}$ and $\mathbf{h}_{k+1|k} = \mathbf{h}(\overline{\mathbf{Z}}_{k+1|k}) - \mathbf{H}_{k+1|k}\overline{\mathbf{Z}}_{k+1|k}$

Here, $\overline{\mathbf{Z}}_{k+1|k}$ can be estimated from equation (4) based on the zero-order hold sampling (ZOH), in which the seismic excitation $\ddot{x}_g(t)$ is assumed constant with a sampling interval as follows:

$$\overline{\mathbf{Z}}_{k+1|k} = \widehat{\mathbf{Z}}_{k|k} + \int_{k\Delta t}^{(k+1)\Delta t}\left[\mathbf{g}\left(\widehat{\mathbf{Z}}_{t|k}\right) + \mathbf{B}\widehat{\ddot{x}}_{g,t|k} + \mathbf{B}^c u_{t|k}\right]\mathrm{d}t. \tag{14}$$

Since there is no direct feedback of the unknown input $\ddot{x}_g(t)$ in the observation equation, the first-order hold (FOH) sampling is used for the unknown seismic excitation $\ddot{x}_g(t)$ in equation (4). Thus, equation (4) is discretized as follows:

$$\mathbf{Z}_{k+1} = \mathbf{A}_k\mathbf{Z}_k + \mathbf{B}_k^u\ddot{x}_{g,k} + \mathbf{B}_{k+1}^u\ddot{x}_{g,k+1} + \mathbf{B}_k^c u_k + \mathbf{g}_{t|k} + \mathbf{w}_k, \tag{15}$$

in which, $\mathbf{A}_k = \mathbf{e}^{\mathbf{G}_{k|k}\Delta t}$; $\mathbf{g}_{k|k} = (\mathbf{A}_k - \mathbf{I})(\mathbf{G}_{k|k}\Delta t)^{-1}[\mathbf{g}(\widehat{\mathbf{Z}}_{k|k}) - \mathbf{G}_{k|k}\widehat{\mathbf{Z}}_{k|k}]\Delta t$;

$$\begin{aligned}\mathbf{B}_k^u &= \left[\mathbf{A}_k - (\mathbf{A}_k - \mathbf{I})(\mathbf{G}_{kk}\Delta t)^{-1}\right]\left(\mathbf{G}_{k|k}\Delta t\right)^{-1}(\mathbf{B}\Delta t);\\ \mathbf{B}_{k+1}^u &= \left[(\mathbf{A}_k - \mathbf{I})\left(\mathbf{G}_{k|k}\Delta t\right)^{-1} - \mathbf{I}\right]\left(\mathbf{G}_{k|k}\Delta t\right)^{-1}(\mathbf{B}\Delta t)\\ \mathbf{B}_k^c &= (\mathbf{A}_k - \mathbf{I})\left(\mathbf{G}_{k|k}\Delta t\right)^{-1}(\mathbf{B}^c\Delta t),\end{aligned} \tag{16}$$

and $\mathbf{w}_k$ denotes the process error assumed as zero mean and covariance matrix $\mathbf{Q}_k$. Since some rows in the partial derivation $\partial g(\mathbf{Z})/\partial \mathbf{Z}|\mathbf{Z} = \widehat{\mathbf{Z}}_{k|k}$ matrix, the moore-Penrose pseudoinverse is adopted here for the term $(\mathbf{G}_{k|k}\Delta t)^{-1}$ and the function *pinv* in MATLAB is used to execute the pseudoinverse in this paper.

Then, the extended structural state and unknown seismic excitation can be identified by the following steps based on the GEKF-UI method, while derivation details can be found in reference [15]:

(1) The estimation of the unknown seismic excitation $\ddot{\hat{x}}_{g,k+1}$ and the Kalman gain matrix $\mathbf{K}_{k+1}$

$$\ddot{\hat{x}}_{g,k+1|k+1} = \mathbf{S}_{k+1}\left[\mathbf{y}_{k+1} - \mathbf{H}_{k+1|k}\left(\mathbf{A}_k\widehat{\mathbf{Z}}_{k|k} + \mathbf{B}_k^u\ddot{\hat{x}}_{g,k|k} + \mathbf{g}_{k|k}\right) - \mathbf{D}^c u_{k|k} - \mathbf{h}_{k+1|k}\right], \tag{17}$$

$$\mathbf{S}_{k+1} = \left[\left(\mathbf{H}_{k+1|k}\mathbf{B}_{k+1}^u + \mathbf{D}^u\right)^T\widetilde{\mathbf{R}}^{-1}\left(\mathbf{H}_{k+1|k}\mathbf{B}_{k+1}^u + \mathbf{D}^u\right)\right]^{-1}\left(\mathbf{H}_{k+1|k}\mathbf{B}_{k+1}^u + \mathbf{D}^u\right)^T\widetilde{\mathbf{R}}^{-1}, \tag{18}$$

$$\widetilde{\mathbf{R}}^{-1} = \left(\mathbf{H}_{k+1|k}\widetilde{\mathbf{P}}_{k+1|k}^{\mathbf{Zp}}\mathbf{H}_{k+1|k}^T + \mathbf{R}_{k+1}\right)^{-1}, \tag{19}$$

$$\mathbf{K}_{k+1} = \widetilde{\mathbf{P}}_{k+1|k}^{\mathbf{Zp}}\mathbf{H}_{k+1|k}^T\left(\mathbf{H}_{k+1}\widetilde{\mathbf{P}}_{k+1|k}^{\mathbf{Zp}}\mathbf{H}_{k+1|k}^T + \mathbf{R}_{k+1}\right)^{-1}. \tag{20}$$

The covariance matrix $\widetilde{\mathbf{P}}_{k+1|k}^{\mathbf{Zp}}$ can be derived as follows:

$$\begin{aligned}\widetilde{\mathbf{P}}_{k+1|k}^{\mathbf{Zp}} &= E\left[\left(\tilde{\mathbf{e}}_{k+1|k}^{\mathbf{Zp}}\right)\left(\tilde{\mathbf{e}}_{k+1|k}^{\mathbf{Zp}}\right)^T\right]\\ &= \begin{bmatrix}\mathbf{A}_k & \mathbf{B}_k\end{bmatrix}\begin{bmatrix}\widehat{\mathbf{P}}_{k|k}^{\mathbf{Z}} & \widehat{\mathbf{P}}_{k|k}^{\mathbf{Zf}}\\ \widehat{\mathbf{P}}_{k|k}^{\mathbf{fZ}} & \widehat{\mathbf{P}}_{k|k}^{\mathbf{f}}\end{bmatrix}\begin{bmatrix}\mathbf{A}_k^T\\ \mathbf{B}_k^T\end{bmatrix} + \mathbf{Q}_k.\end{aligned} \tag{21}$$

(2) The prediction and estimation of the extended stat vector are

$$\widetilde{\mathbf{Z}}_{k+1|k} = \mathbf{A}_k\widehat{\mathbf{Z}}_{k|k} + \mathbf{B}_k^u\ddot{\hat{x}}_{g,k|k} + \mathbf{B}_{k+1}^u\ddot{\hat{x}}_{g,k+1|k+1} + \mathbf{B}_k^c u_{k|k} + \mathbf{g}_{k|k}, \tag{22}$$

$$\widehat{\mathbf{Z}}_{k+1|k+1} = \widetilde{\mathbf{Z}}_{k+1|k} + \mathbf{K}_{k+1}\left[\mathbf{y}_{k+1} - \mathbf{H}_{k+1|k}\widetilde{\mathbf{Z}}_{k+1|k} - \mathbf{D}^c u_{k|k} - \mathbf{h}_{k+1|k}\right]. \tag{23}$$

Different from the estimated $\overline{\mathbf{Z}}_{k+1|k}$ in equation (14), $\widetilde{\mathbf{Z}}_{k+1|k}$ in equation (22) is estimated from the linearized state equation of equation (15). The corresponding covariance matrices can be derived as follows:

$$\widehat{\mathbf{P}}^{\mathbf{f}}_{k+1|k+1} = E\left[\left(\widehat{\mathbf{e}}^{\mathbf{f}}_{k+1|k+1}\right)\left(\widehat{\mathbf{e}}^{\mathbf{f}}_{k+1|k+1}\right)^T\right] = \mathbf{S}_{k+1}\left(\mathbf{H}_{k+1|k}\widehat{\mathbf{P}}^{\mathbf{Z}}_{k+1|k}\mathbf{H}^T_{k+1|k} + \mathbf{R}\right)\mathbf{S}^T_{k+1}, \tag{24}$$

$$\widehat{\mathbf{P}}^{\mathbf{Zf}}_{k+1|k+1} = \left(\widehat{\mathbf{P}}^{\mathbf{fZ}}_{k+1|k+1}\right)^T = E\left[\left(\widehat{\mathbf{e}}^{\mathbf{Z}}_{k+1|k+1}\right)\left(\widehat{\mathbf{e}}^{\mathbf{f}}_{k+1|k+1}\right)^T\right] = -\left[\mathbf{K}_{k+1}\left(\mathbf{H}_{k+1|k}\mathbf{B}_{k+1} + \mathbf{D}\right) - \mathbf{B}_{k+1}\right]\widehat{\mathbf{P}}^{\mathbf{f}}_{k+1|k+1}, \tag{25}$$

$$\begin{aligned}\mathbf{P}^{\mathbf{Z}}_{k+1|k+1} &= E\left[\left(\widehat{\mathbf{e}}^{\mathbf{Z}}_{k+1|k+1}\right)\left(\widehat{\mathbf{e}}^{\mathbf{Z}}_{k+1|k+1}\right)^T\right] \\ &= \left(\mathbf{I} - \mathbf{K}_{k+1}\mathbf{H}_{k+1|k}\right)\widehat{\mathbf{P}}^{\mathbf{Z}}_{k+1|k} + \left[\mathbf{K}_{k+1}\left(\mathbf{H}_{k+1|k}\mathbf{B}_{k+1} + \mathbf{D}^u\right) - \mathbf{B}_{k+1}\right]\widehat{\mathbf{P}}^{\mathbf{f}}_{k+1|k+1}\left[\mathbf{K}_{k+1}\left(\mathbf{H}_{k+1|k}\mathbf{B}_{k+1} + \mathbf{D}^u\right) - \mathbf{B}_{k+1}\right]^T.\end{aligned} \tag{26}$$

2.3. Real Time Integration with Semiactive Optimization Vibration Control Algorithm. In this paper, the linear-quadratic regulator (LQR) control algorithm is adopted for the optimal vibration control of the system. Then, the optimal active control force is determined by

$$u^{lqg} = -\mathbf{G}\mathbf{Z}^c, \tag{27}$$

where $\mathbf{Z}^c = [\mathbf{x}\,\dot{\mathbf{x}}]^T$ is structural state vector; $\mathbf{G} = \mathbf{R}^c\mathbf{E}^T\mathbf{P}$ is the optimal control force feedback matrix; $\mathbf{E} = \begin{bmatrix}\mathbf{0}\\ \mathbf{M}^{-1}\boldsymbol{\eta}^c\end{bmatrix}$. Here, $\mathbf{P}$ can be derived by solving the following Riccati equation:

$$\mathbf{P}\mathbf{H}^c + \left(\mathbf{H}^c\right)^T\mathbf{P} - \mathbf{P}\mathbf{E}\left(\mathbf{R}^c\right)^{-1}\left(\mathbf{E}\right)^T\mathbf{P} + \mathbf{Q}^c = 0, \tag{28}$$

where $\mathbf{H}^c = \begin{bmatrix}\mathbf{0} & \mathbf{I}\\ -\mathbf{M}^{-1}\mathbf{K} & -\mathbf{M}^{-1}\mathbf{C}\end{bmatrix}$; Qc and Rc are two weighting matrices of the LQG control performance index [3]. In this paper, they are selected as $\mathbf{Q}^c = \alpha\begin{bmatrix}\mathbf{K} & \mathbf{0}\\ \mathbf{0} & \mathbf{C}\end{bmatrix}$ and $\mathbf{R}^c = \beta\mathbf{I}$.

With the identified results of input-parameters-state of the SAMD-building combined system in Sections 2.1 and 2.2, optimal vibration control of the combined system can be integrated in real time. The optimal active control force is determined from equation (27) by

$$\widehat{u}^{lqg}_{k+1|k+1} = -\mathbf{G}_{k+1}\widehat{\mathbf{Z}}^c_{k+1|k+1}, \tag{29}$$

where $\widehat{\mathbf{Z}}^c_{k+1|k+1} = [\widehat{\mathbf{x}}_{k+1|k+1}\,\widehat{\dot{\mathbf{x}}}_{k+1|k+1}]^T$, $\mathbf{G}_{k+1}$ is the feedback matrix of control force determined by

$$\mathbf{G}_{k+1} = \mathbf{R}^c\mathbf{E}^T\mathbf{P}_{k+1}, \tag{30}$$

and $\mathbf{P}_{k+1}$ is the solution of the Riccati equation as follows:

$$\mathbf{P}_{k+1}\mathbf{H}^c_{k+1} + \left(\mathbf{H}^c_{k+1}\right)^T\mathbf{P}_{k+1} - \mathbf{P}_{k+1}\mathbf{E}\left(\mathbf{R}^c\right)^{-1}\left(\mathbf{E}\right)^T\mathbf{P}_{k+1} + \mathbf{Q}^c_{k+1} = 0, \tag{31}$$

where

$$\mathbf{H}^c_{k+1} = \begin{bmatrix}\mathbf{0} & \mathbf{I}\\ -\mathbf{M}^{-1}\mathbf{K}\left(\widehat{\boldsymbol{\theta}}_{k+1|k+1}\right) & -\mathbf{M}^{-1}\mathbf{C}\left(\widehat{\boldsymbol{\theta}}_{k+1|k+1}\right)\end{bmatrix}; \mathbf{Q}^c_{k+1} = \alpha\begin{bmatrix}\mathbf{K}\left(\widehat{\boldsymbol{\theta}}_{k+1|k+1}\right) & \mathbf{0}\\ \mathbf{0} & \mathbf{C}\left(\widehat{\boldsymbol{\theta}}_{k+1|k+1}\right)\end{bmatrix}. \tag{32}$$

Furthermore, for the semiactive optimization vibration control with MR damper, the semiactive optimization control force is determined by [15, 16]

$$u(t) = c\dot{y}(t) + f_{dy}\mathrm{sgn}[\dot{y}(t)], \tag{33}$$

where c and f_{dy} are the viscous damping coefficient and the adjustable coulomb damping force of the MR damper, respectively, and $\dot{y}(t)$ is the relative velocity of the MR damper.

By using the estimated state values at time instant $(k+1)\Delta t$, the Hrovat semiactive control strategy is adopted to realize the transformation from optimal active control force to semiactive optimization control force according to [15, 16]:

$$\widehat{u}_{k+1|k+1} = \begin{cases} c\widehat{\dot{y}}_{k+1|k+1} + f^{\max}_{dy}\mathrm{sgn}\left[\widehat{\dot{y}}_{k+1|k+1}\right], & \widehat{u}^{lqg}_{k+1|k+1}\cdot\widehat{\dot{y}}_{k+1|k+1} < 0\ and\ \left|\widehat{u}^{lqg}_{k+1|k+1}\right| > \widehat{u}^{\max}_{k+1|k+1},\\ \left|\widehat{u}^{lqg}_{k+1|k+1}\right|\mathrm{sgn}\left[\widehat{\dot{y}}_{k+1|k+1}\right], & \widehat{u}^{lqg}_{k+1|k+1}\cdot\widehat{\dot{y}}_{k+1|k+1} < 0\ and\ \left|\widehat{u}^{lqg}_{k+1|k+1}\right| < \widehat{u}^{\max}_{k+1|k+1},\\ c\widehat{\dot{y}}_{k+1|k+1} + f^{\min}_{dy}\mathrm{sgn}\left[\widehat{\dot{y}}_{k+1|k+1}\right], & \widehat{u}^{lqg}_{k+1|k+1}\cdot\widehat{\dot{y}}_{k+1|k+1} > 0, \end{cases} \tag{34}$$

where $f_{dy}^{\max}$ and $f_{dy}^{\min} = 0$ denote the maximum and minimum coulomb damping forces, respectively, $\hat{u}_{k+1|k+1}^{\max} = c|\hat{\dot{y}}_{k+1|k+1}| + f_{dy}^{\max}$ is the maximum damping force provided by the MR damper, $\hat{u}_{k+1|k+1}^{lqg}$ is the desirable optimal control force obtained from LQR control algorithm, c and $f_{dy}^{\max}$ are the two constants related to the MR damper device, which can be determined based on the relevant design approach [15, 16], and $\hat{\dot{y}}_{k+1|k+1}$ is the estimated relative velocity of MR damper, which can be obtained from the estimated state vector $\hat{\mathbf{Z}}_{k+1|k+1}$ in equation (8) or equation (23).

In summary, the flowchart of the proposed real-time integration of identification and semiactive optimization vibration control for mass damper-building combined systems under known/unknown seismic excitations is shown in Figure 2.

3. Numerical Simulation Validations

As shown in Figure 3, a ten-story shear frame structure equipped with a SAMD using a magnetic rheology damper (MR) on the top floor is used. The parameters of the SAMD-frame combined system are shown in Table 1. The frame is excited by the EI-Centrol earthquake.

For the SMAD-shear frame combined system, the mass, damping, and stiffness matrices of the system can be constructed from equations (2) and (3) as follows:

$$\mathbf{M} = \begin{bmatrix} m_1 & 0 & \cdots & 0 & 0 \\ 0 & m_2 & \ddots & \vdots & 0 \\ \vdots & \ddots & \ddots & 0 & \vdots \\ 0 & \cdots & 0 & m_{10} & 0 \\ 0 & 0 & \cdots & 0 & m_s \end{bmatrix}; \mathbf{C} = \begin{bmatrix} c_1 + c_2 & -c_2 & \cdots & 0 & 0 \\ -c_2 & c_2 + c_3 & \ddots & \vdots & 0 \\ \vdots & \ddots & \ddots & -c_{10} & \vdots \\ 0 & \cdots & -c_{10} & c_{10} + c_s & -c_s \\ 0 & 0 & \cdots & -c_s & c_s \end{bmatrix}; \mathbf{K} = \begin{bmatrix} k_1 + k_2 & -k_2 & \cdots & 0 & 0 \\ -k_2 & k_2 + k_3 & \ddots & \vdots & 0 \\ \vdots & \ddots & \ddots & -k_{10} & \vdots \\ 0 & \cdots & -k_{10} & k_{10} + k_s & -k_s \\ 0 & 0 & \cdots & -k_s & k_s \end{bmatrix}. \quad (35)$$

It should be mentioned that the mass coefficients m_i and m_s are assumed known, while the damping and stiffness coefficients c_i, k_i, c_s, and k_s are unknown. The initial values of the unknown parameters are selected as 80% of their real values in implementing the EKF or GEKF-UI algorithm.

The LQR control algorithm is used for the optimal active control force u^{lqg}, and the two control coefficients α and β in equation (28) are set as $\alpha = 50$ and $\beta = 10^{-2}$ for the following two cases.

To evaluate the control performance, two sets of performance indicators are used [26]. The first set of indicators contains the peak and RMS ratios based on interstory displacement (J_1 and J_3), the peak and RMS ratios based on absolute acceleration response (J_2 and J_4), expressed as follows:

$$J_1 = \left\{ \frac{\max_{t,j} |dx_i(t)|/h_i}{\delta^{\max}} \right\}; J_2 = \left\{ \frac{\max_{t,j} |x_{ai}(t)|}{\ddot{x}_a^{\max}} \right\}; J_3 = \left\{ \frac{\max_{t,j} \|dx_i(t)\|/h_i}{\|\delta^{\max}\|} \right\}; J_4 = \left\{ \frac{\max_{t,j} \|x_{ai}(t)\|}{\|\ddot{x}_a^{\max}\|} \right\}, \quad (36)$$

in which, $dx_i(t)$ represents the i-th interstory displacement of the controlled structure; h_i indicates the level i-story height; $\delta^{\max}$ represents the maximum interstory displacement ratio of the uncontrolled structure; $\ddot{x}_{ai}$ is absolute acceleration response of story i-th controlled structure; $\ddot{x}_a^{\max}$ is the maximum acceleration response of the uncontrolled structure; the RMS values in J_3 and J_4 can be gain by $\|\bullet\| = \sqrt{(1/t_f)\int_0^{t_f} [\bullet]^2 \mathrm{dt}}$; $\max_{t,j}$ denotes the maximum across all floors at al time points.

The second set of performance indicators are related to the performance of the control device. In this paper, only the peak-based control force is selected, which is expressed as follows:

$$J_5 = \left\{ \frac{\max_{t,j} |f_i(t)|}{W} \right\}, \quad (37)$$

in which, $f_i(t)$ is the control force provided by the control equipment in the i-th story; W is the representative value of building gravity load, in this paper is the sum of gravity for each floor.

3.1. SAMD-Frame Combined System under Known Seismic Excitation. In this case, relative acceleration responses at the 1st, 3rd, 5th, 6th, 7th, and 10th floor levels are observed and measurement noise with 5% noise-signal ratio in root mean square (RMS) is considered.

Figure 4 shows that the acceleration and displacement responses of the frame with SAMD (with SAMD) on the top story are significantly smaller than those of the frame without SAMD (w/o SAMD).

As shown in Figure 5, the stiffness and damping parameters of the SAMD quickly converge to the true values.

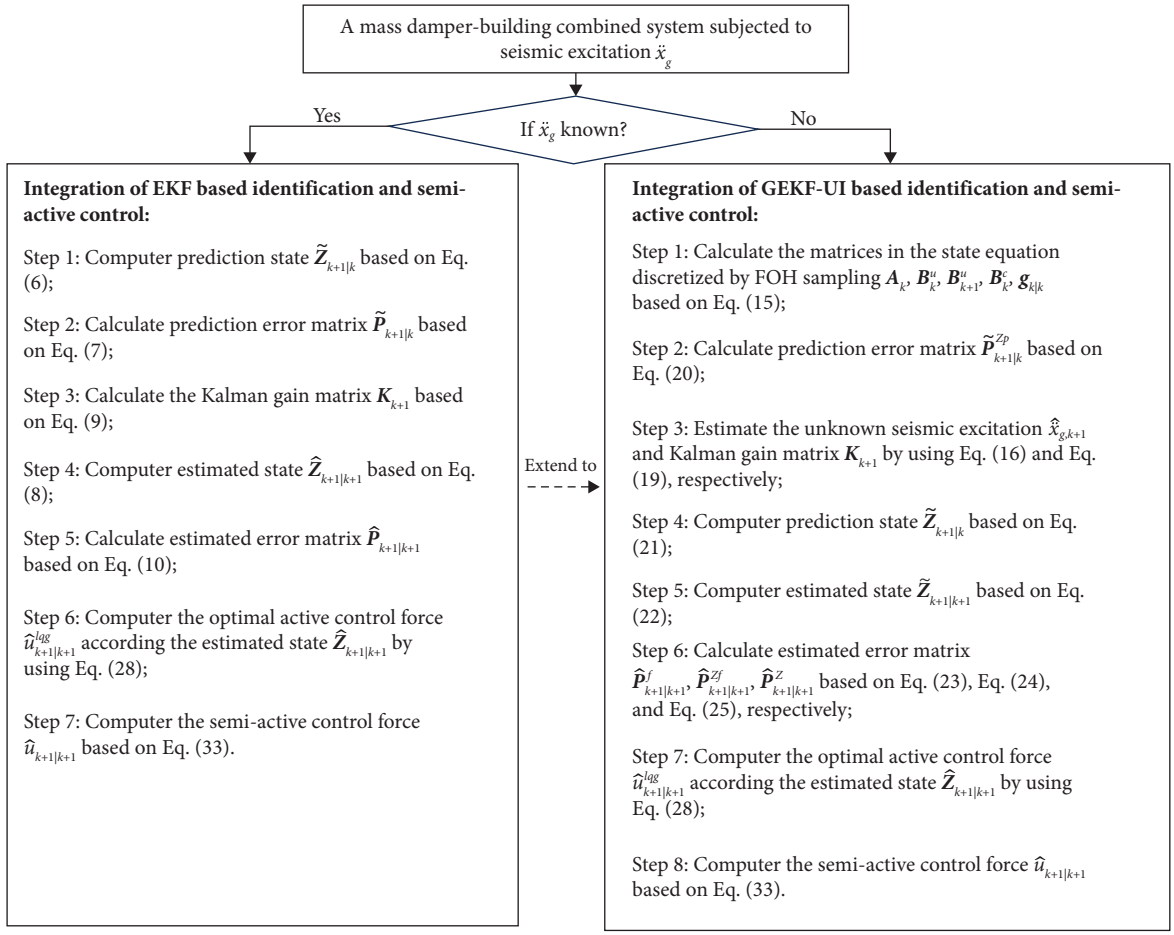

Figure 2: Flow chart of the proposed real-time integration method.

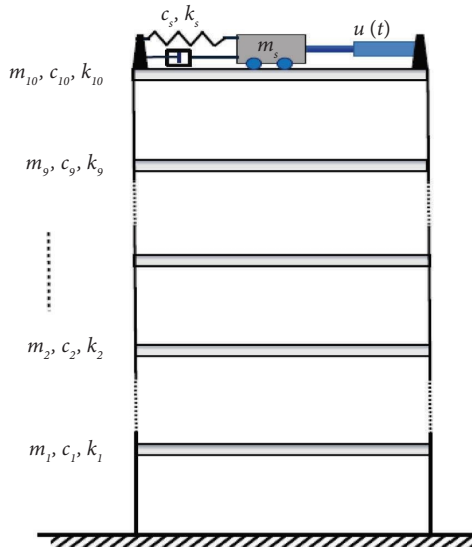

Figure 3: The SAMD-building model in numerical validations.

Table 2 summarizes the identified stiffness parameters of the SAMD-building combined system, and the identification errors are small. Table 3 shows the comparisons of the identified damping coefficients of the combined system.

Table 1: Parameters of the SAMD-frame combined system.

Parameter	Value
m_i $(i = 1, 2, \ldots, 10)$	6000 kg
k_i $(i = 1, 2, \ldots, 10)$	1.2×10^3 N/m
c_i $(i = 1, 2, \ldots, 10)$	6×10^3 N•sec /m
m_s	360 kg
k_s	1.2×10^3 N/m
c_s	100 N•sec /m

Although the identification accuracy is inferior, the errors are mostly within 5%.

Figure 6 shows the time histories of the top floor responses and the control force. The solid curves with legend of "Integrated" represent the results obtained from the proposed integrated method, while the dash curves with legend of "Control" represent the results obtained from the conventional optimal control algorithm.

Figure 7 compares the maximum values of story acceleration, displacements and drifts by the proposed integrated method and the conventional optimal control algorithm. Form these comparisons in Figures 6 and 7, it is shown that structural responses by the proposed integrated method are consistent with the conventional semiactive optimization control algorithm.

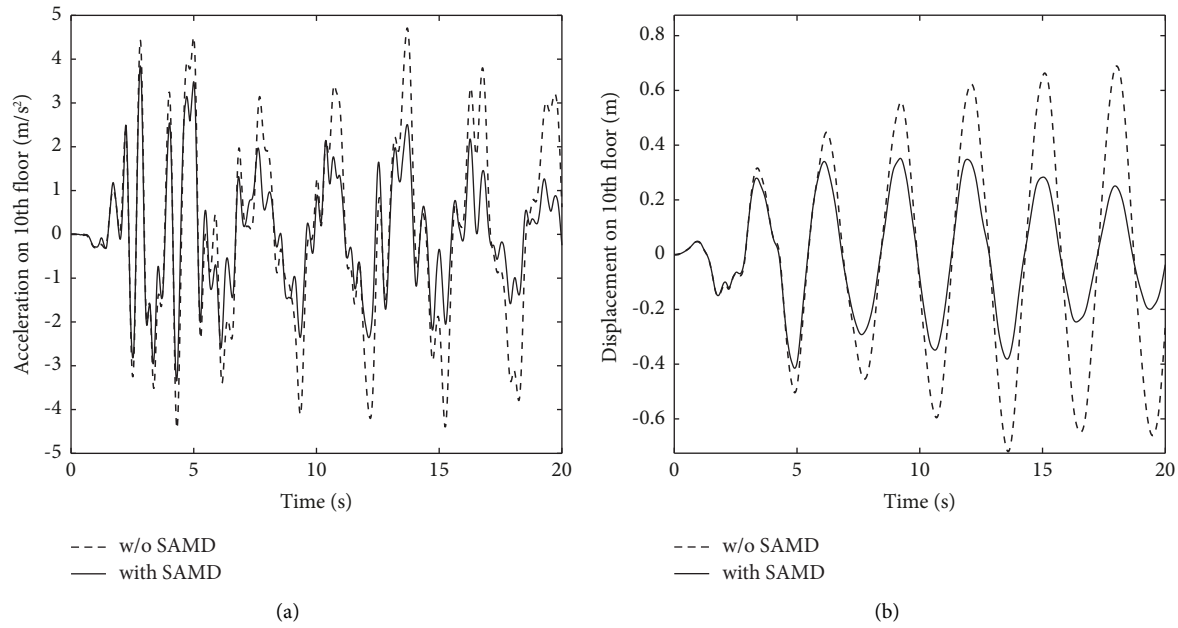

Figure 4: Structural responses with and without SAMD (known seismic excitation). (a) Acceleration response. (b) Displacement response.

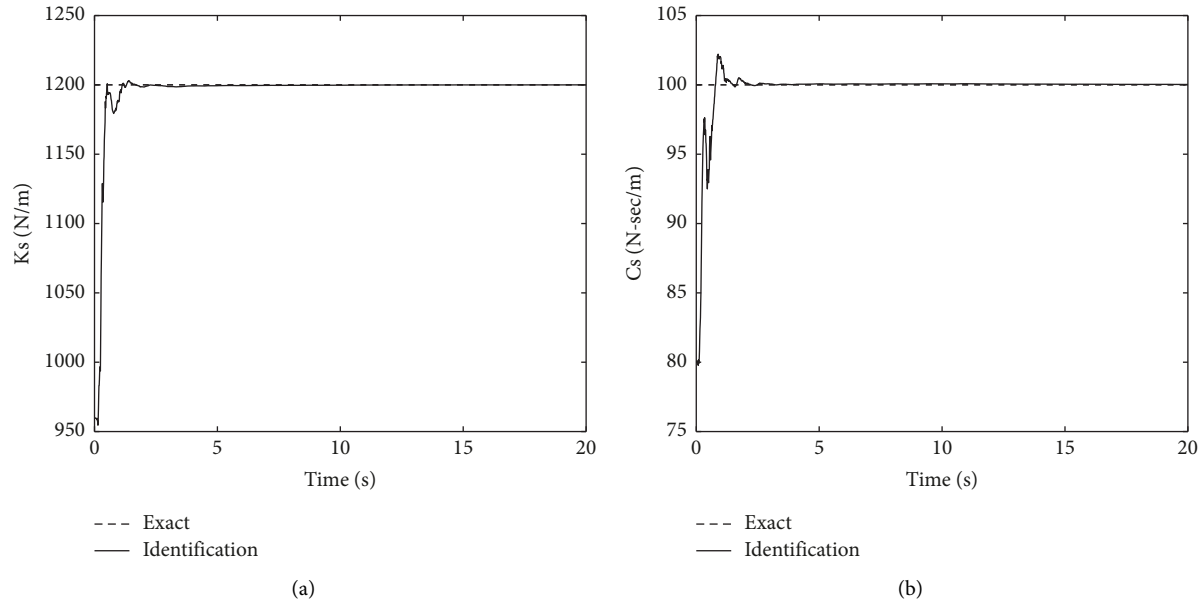

Figure 5: The identified SAMD parameters (known seismic excitation). (a) Stiffness parameter k_s. (b) Damping parameter c_s.

Table 4 shows the comparisons of control performance indicators $J_1 - J_5$ by the proposed integrated method and the conventional optimal control algorithm. It is demonstrated that the proposed integrated method can reach almost the same optimal control effects as the conventional control.

3.2. SAMD-Frame Combined System under Unknown Seismic Excitation. In this case, absolute acceleration responses at the 1st, 3rd, 5th, 6th, 7th, and 10th floor levels are observed. Moreover, fusion with the interstory displacement between the 1st floor and the ground is used to overcome the identification drift. Also, measurement noise with 5% noise-signal ratio in root mean square (RMS) is considered.

Figure 8 shows the identified stiffness and damping parameters of the SAMD and Tables 5 and 6 summarizes the identified stiffness and damping parameters of the combined system, respectively. The comparisons presented in Figure 8 and Tables 5 and 6 indicate that the identification errors remain small in the scenario that seismic excitation is unknown.

Table 2: Comparisons of identified stiffness parameters (known seismic excitation).

Story no	Exact (103 N/m)	Identified (103 N/m)	Error (%)
1st	1200	1205.38	−0.45
2nd	1200	1198.03	0.16
3rd	1200	1202.10	−0.18
4th	1200	1196.34	0.30
5th	1200	1201.51	−0.13
6th	1200	1192.49	0.63
7th	1200	1200.38	−0.03
8th	1200	1197.69	0.19
9th	1200	1203.68	−0.31
10th	1200	1196.76	0.27
SAMD	1.2	1.20	0.00

Table 3: Comparisons of identified damping coefficients (known seismic excitation).

Story no	Exact (N/m)	Identified c (N/m)	Error (%)
1st	6000	6062.19	−1.04
2nd	6000	6000.28	0.00
3rd	6000	6155.54	−2.59
4th	6000	6162.43	−2.71
5th	6000	6247.43	−4.12
6th	6000	5546.10	7.56
7th	6000	5907.44	1.54
8th	6000	5789.72	3.50
9th	6000	6159.76	−2.66
10th	6000	5962.92	0.62
SAMD	100	100.09	−0.10

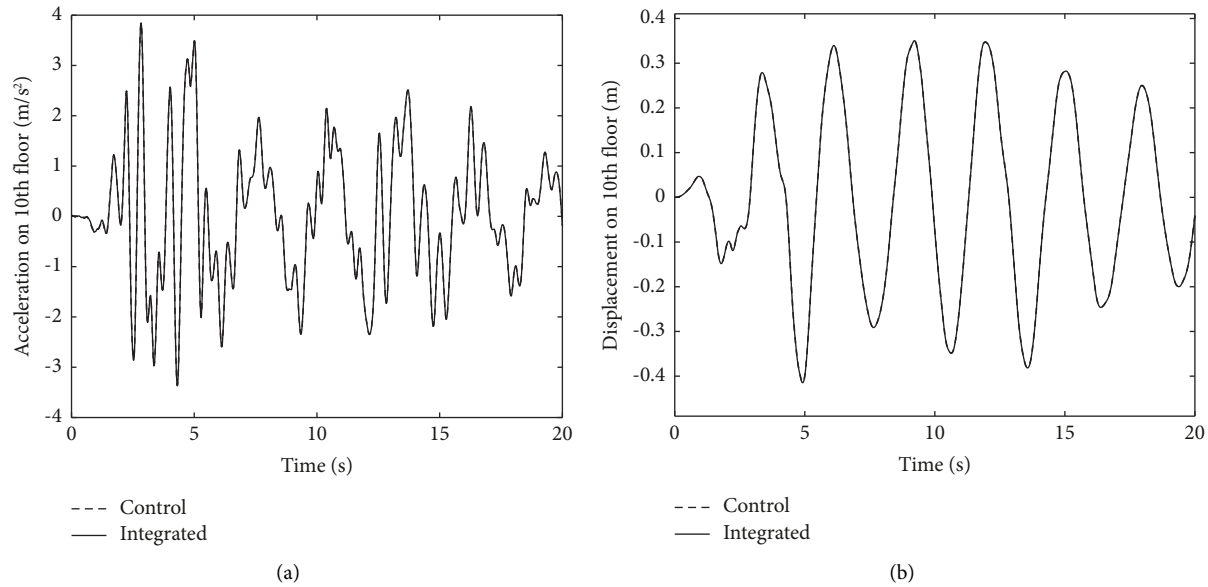

Figure 6: Continued.

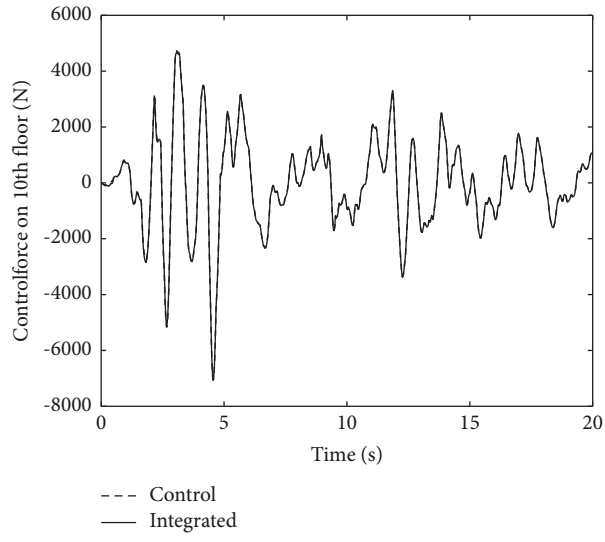

(c)

Figure 6: Responses and control force by integrated and control method (known seismic excitation). (a) Acceleration of the top floor. (b) Displacement of the top floor. (c) Control force at the top floor.

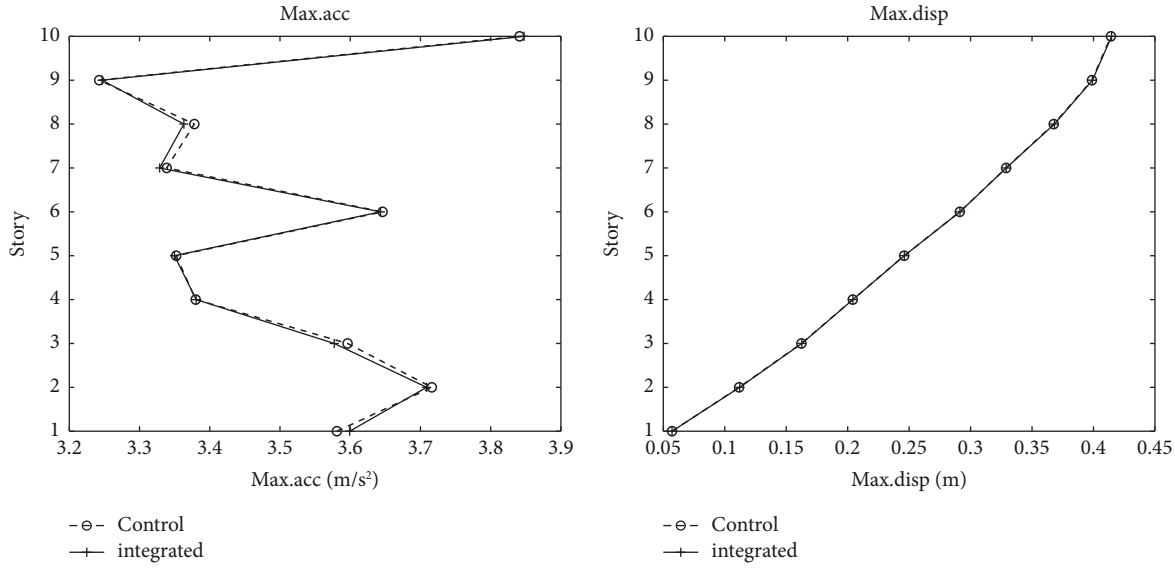

(a) (b)

Figure 7: Continued.

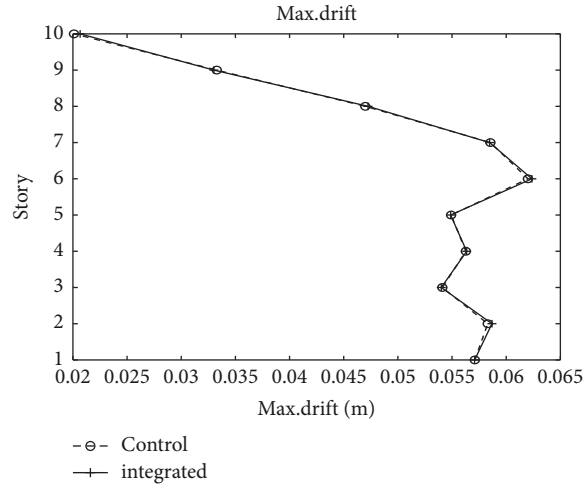

(c)

Figure 7: Maximum story accelerations, displacements, and drifts (known seismic excitation). (a) Maximum story acceleration responses. (b) Maximum story displacement responses. (c) Maximum interstory displacement responses.

Table 4: Control performance indicators (known seismic excitation).

Performance indices	Integrated identification and control	Conventional control
J_1 (peak story drift ratio)	0.633	0.632
J_2 (peak acc.)	0.814	0.815
J_3 (rms drift ratio)	0.542	0.541
J_4 (rms acc.)	0.626	0.626
J_5 (control force)	0.012	0.012

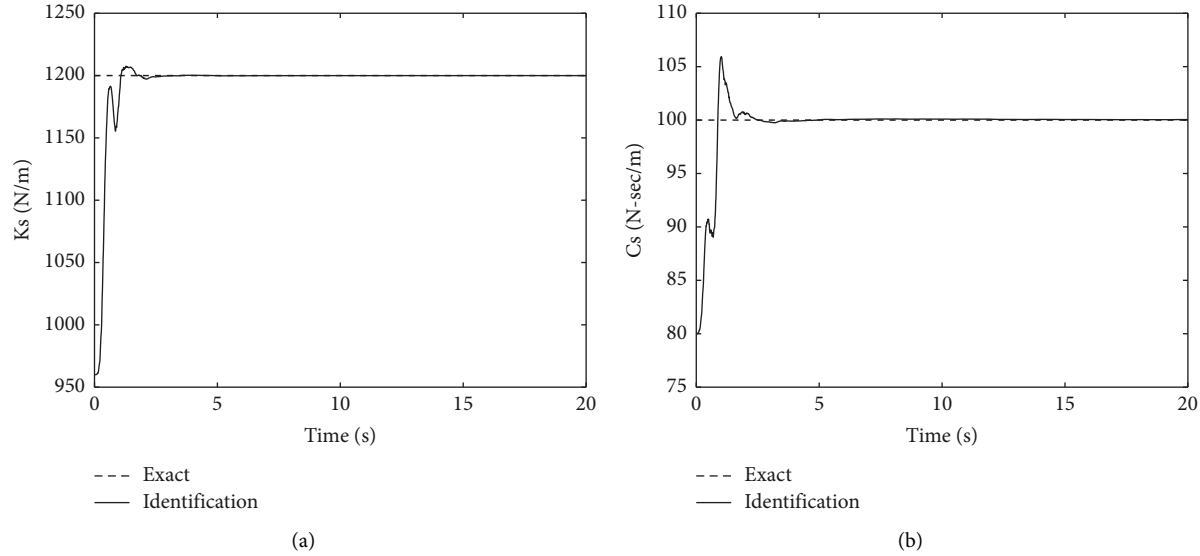

(a) (b)

Figure 8: The identified SAMD parameters (unknown seismic excitation). (a) Stiffness coefficient. (b) Damping coefficient.

Figure 9 presents a comparison of the time histories of structural acceleration, displacement response, and control force at the top floor. This comparison is conducted between the proposed integrated method and the conventional optimal control algorithm.

Likewise, Figure 10 provides a detailed comparison of the maximum values of story accelerations, displacements, and drifts obtained through the proposed integrated method and the traditional optimal control algorithm.

Table 5: Comparisons of identified stiffness coefficients (unknown seismic excitation).

Story no	Exact (103 N/m)	Identified (103 N/m)	Error (%)
1st	1200	1200.78	−0.07
2nd	1200	1198.66	0.11
3rd	1200	1197.31	0.22
4th	1200	1199.50	0.04
5th	1200	1197.75	0.19
6th	1200	1199.15	0.07
7th	1200	1201.87	−0.16
8th	1200	1200.91	−0.08
9th	1200	1200.57	−0.05
10th	1200	1203.40	−0.28
SAMD	1.2	1.19	0.00

Table 6: Comparisons of identified damping coefficients (unknown seismic excitation).

Story no	Exact (N/m)	Identified c (N/m)	Error (%)
1st	6000	6002.02	−0.03
2nd	6000	6130.07	−2.17
3rd	6000	6067.38	−1.12
4th	6000	5946.77	0.89
5th	6000	5761.88	3.97
6th	6000	6001.38	−0.02
7th	6000	5889.00	1.85
8th	6000	5900.95	1.65
9th	6000	6281.78	−4.70
10th	6000	6073.32	−1.22
SAMD	100	100.04	−0.05

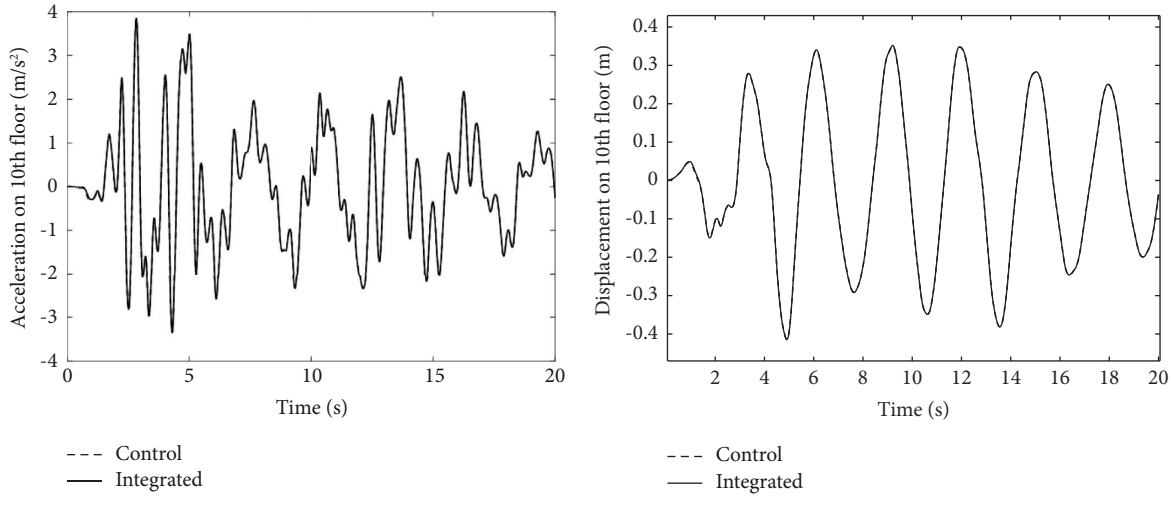

Figure 9: Continued.

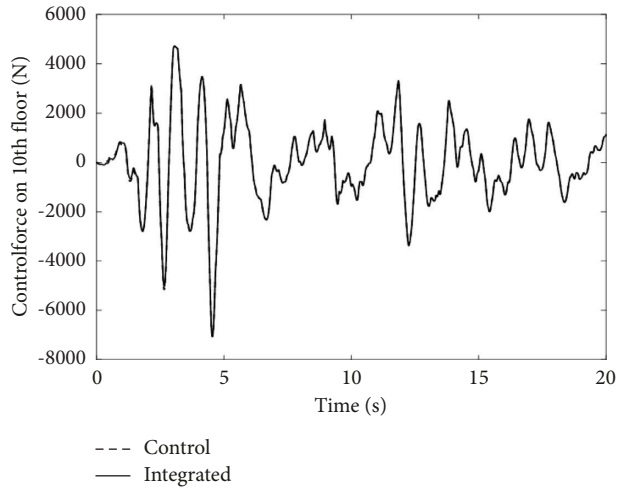

(c)

Figure 9: Responses and control force by integrated and control method (unknown seismic excitation). (a) Acceleration of the top floor. (b) Displacement of the top floor. (c) Control force at the top floor.

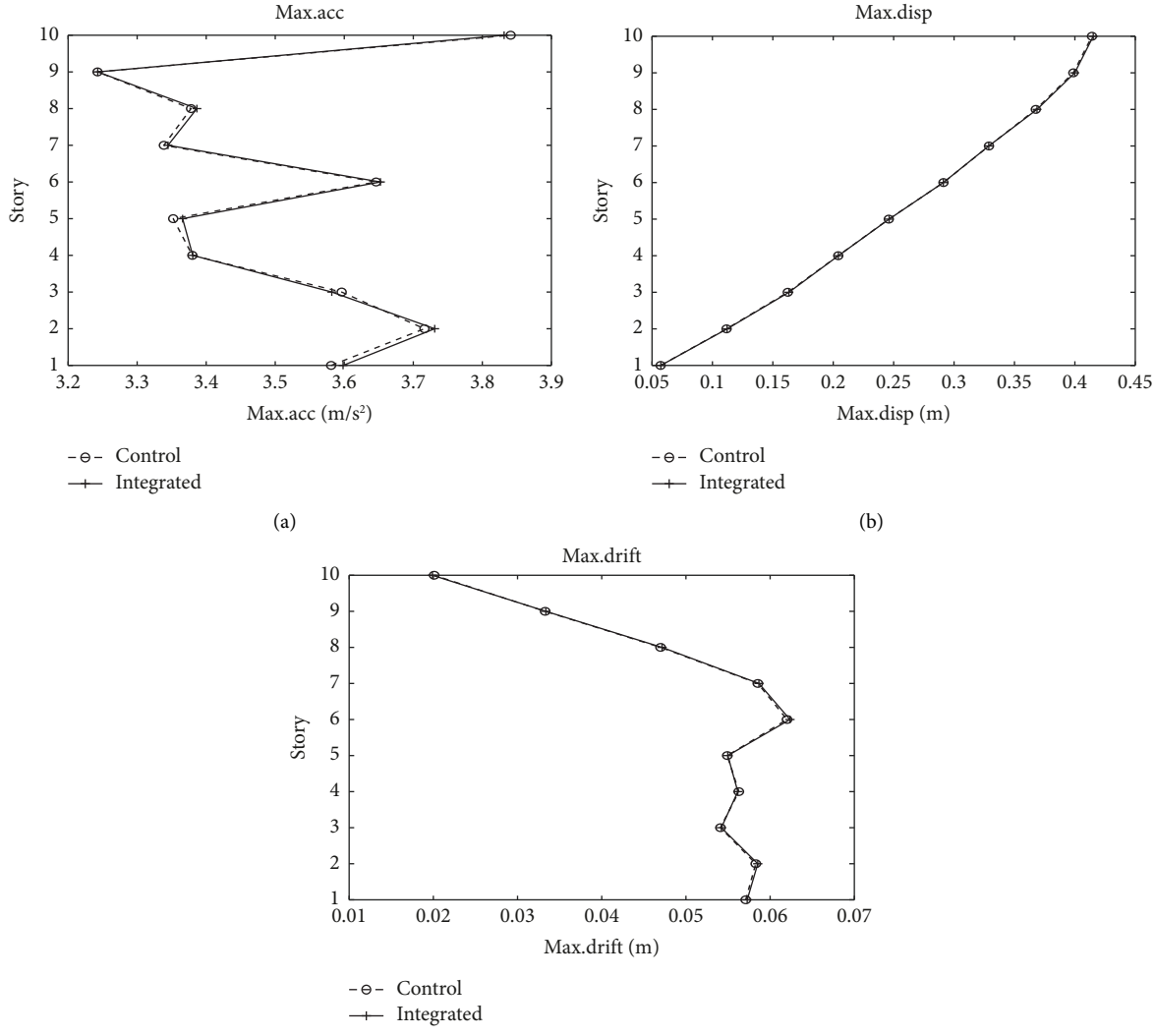

Figure 10: Maximum story accelerations, displacements and drifts (unknown seismic excitation). (a) Maximum story acceleration responses. (b) Maximum story displacement responses. (c) Maximum interstory displacement responses.

Table 7: Control performance indicators (unknown seismic excitation).

Performance indices	Integrated control and identification	Conventional control
J_1 (peak story drift ratio)	0.633	0.632
J_2 (peak acc.)	0.814	0.815
J_3 (rms drift ratio)	0.542	0.541
J_4 (rms acc.)	0.626	0.626
J_5 (control force)	0.012	0.012

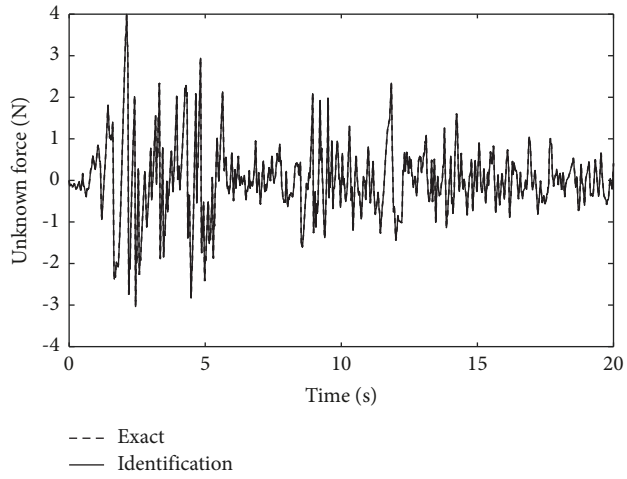

Figure 11: Comparison of the identified unknown seismic excitation.

The key takeaway from these comparisons is that the structural responses achieved through the proposed integrated method are consistent with the conventional semiactive optimization control algorithm. This alignment demonstrates the effectiveness of the integrated approach and indicates that it can maintain structural performance in a manner consistent with the established control methods.

Then, the control performance indicators J_1–J_5 by the proposed integrated method are compared with those by the conventional control algorithm in Table 7. Again, it is shown that the proposed integrated method can reach almost the same optimal control effects by the conventional control in this case of unknown seismic excitation.

Finally, Figure 11 shows the comparison of the identified seismic excitation and its true values. It can be seen that the proposed method can also identify the unknown seismic excitation.

4. Conclusions

Although there are studies on the integration of structural identification and vibration optimal control, there is a lack of integrated identification of mass damper-structure combined systems and semiactive optimization control of the structural systems. This paper proposes a methodology for real-time integration of identification and semiactive optimization vibration control for mass damper-building combined systems under known/unknown seismic excitations. Only partial measurements of structural responses are needed and the seismic excitations can be known or unknown. The identification results of the SADM-building combined system are integrated in real time with the semiactive optimization control algorithm. Numerical simulation examples validate that the proposed integrated identification and semiactive optimization control can reach almost the same optimal control effects by the conventional control with known structural parameters of the mass damper-structure systems under known seismic excitations.

In this paper, the proposed integration methodology is demonstrated by the integrated identification of control of a SAMD on a shear frame structure. Further studies on the validation of the proposed method for building or bridge structures with complex configurations are needed. In addition, this paper only investigates the integrated identification and semiactive optimization control of SAMD-structure systems under seismic excitations; it is required to explore the integrated identification and control of SAMD-building combined system under wind loads. These studies are undertaken by the authors.

Data Availability

All data used in the study are available from the corresponding author upon reasonable request.

Conflicts of Interest

The authors declare that they have no conflicts of interest.

Acknowledgments

The research in this paper is supported by the Key Program of the National Natural Science Foundation of China through the Grant no. 51838006.

References

[1] J. P. Ou and H. Li, "Structural health monitoring in mainland China: review and future trends," *Structural Health Monitoring*, vol. 9, no. 3, pp. 19–231, 2010.

[2] W. Fan and P. Z. Qiao, "Vibration-based damage identification methods: a review and comparative study," *Structural Health Monitoring*, vol. 10, no. 1, pp. 83–111, 2011.

[3] F. Casciati, J. Rodellar, and U. Yildirim, "Active and semiactive control of structures-theory and applications: a review of recent advances," *Journal of Intelligent Material Systems and Structures*, vol. 23, no. 11, pp. 1181–1195, 2012.

[4] J. P. Amezquita-Sanchez, A. Dominguez-Gonzalez, R. Sedaghati, R. de Jesus Romero-Troncoso, and R. A. Osornio-Rios, "Vibration control on smart civil structures: a review," *Mechanics of Advanced Materials and Structures*, vol. 21, no. 1, pp. 23–38, 2014.

[5] Y. L. Xu, Q. Huang, Y. Xia, and H. J. Liu, "Integration of health monitoring and vibration control for smart building structures with time-varying structural parameters and unknown excitations," *Smart Structures and Systems*, vol. 15, no. 3, pp. 807–830, 2015.

[6] Y. Lei, J. B. Lu, and J. S. Huang, "Synthesize identification and control for smart structures with time-varying parameters under unknown earthquake excitation," *Structural Control and Health Monitoring*, vol. 27, no. 4, 2020.
[7] V. Gattulli and F. Romeo, "Integrated procedure for identification and control of MDOF structures," *Journal of Engineering Mechanics*, vol. 126, no. 7, pp. 730–737, 2000.
[8] D. C. Sun and L. Y. Tong, "Closed-loop based detection of debonding of piezoelectric actuator patches in controlled beams," *International Journal of Solids and Structures*, vol. 40, no. 10, pp. 2449–2471, 2003.
[9] H. T. Yang, J. Shan, C. J. Randall, P. K. Hansma, and W. Shi, "Integration of health monitoring and control of building structures during earthquakes," *Journal of Engineering Mechanics*, vol. 140, no. 5, Article ID 04014013, 2014.
[10] Y. Lei, H. Zhou, and L. J. Liu, "An on-line integration technique for structural damage detection and active optimal vibration control," *International Journal of Structural Stability and Dynamics*, vol. 14, no. 05, Article ID 1440003, 2014.
[11] B. Chen, Y. L. Xu, and X. Zhao, "Integrated vibration control and health monitoring of building structures: a time-domain approach," *Smart Structures and Systems*, vol. 6, no. 7, pp. 811–833, 2010.
[12] Q. Huang, Y. L. Xu, J. C. Li, Z. Q. Su, and H. J. Liu, "Structural damage detection of controlled building structures using frequency response functions," *Journal of Sound and Vibration*, vol. 331, no. 15, pp. 3476–3492, 2012.
[13] J. He, Y. L. Xu, S. Zhan, and Q. Huang, "Structural control and health monitoring of building structures with unknown ground excitations: experimental investigation," *Journal of Sound and Vibration*, vol. 390, pp. 23–38, 2017.
[14] J. He, Q. Huang, and Y. L. Xu, "Synthesis of vibration control and health monitoring of building structures under unknown excitation," *Smart Materials and Structures*, vol. 23, no. 10, Article ID 105025, 2014.
[15] Y. Lei, J. B. Lu, J. S. Huang, and S. Chen, "A general synthesis of identification and vibration control of building structures under unknown excitations," *Mechanical Systems and Signal Processing*, vol. 143, Article ID 106803, 2020.
[16] Y. Lei, J. B. Lu, and J. S. Huang, "Integration of identification and vibration control of time-varying structures subject to unknown seismic ground excitation," *Journal of Vibration and Control*, vol. 26, no. 15-16, pp. 1330–1344, 2020.
[17] S. Nagarajaiah, "Adaptive passive, semiactive, smart tuned mass dampers: identification and control using empirical mode decomposition, Hilbert transform, and short-term Fourier transform," *Structural Control and Health Monitoring*, vol. 16, no. 7-8, pp. 800–841, 2009.
[18] P. Y. Lin, L. L. Chung, and C. H. Loh, "Semiactive control of building structures with semiactive tuned mass damper," *Computer-Aided Civil and Infrastructure Engineering*, vol. 20, no. 1, pp. 35–51, 2005.
[19] Y. L. Xu and B. Chen, "Integrated vibration control and health monitoring of building structures using semi-active friction dampers: Part I—methodology," *Engineering Structures*, vol. 30, no. 7, pp. 1789–1801, 2008.
[20] B. Chen and Y. L. Xu, "Integrated vibration control and health monitoring of building structures using semi-active friction dampers: Part II—numerical investigation," *Engineering Structures*, vol. 30, no. 3, pp. 573–587, 2008.
[21] S. Simon and A. Okyay, "Identification and semi-active control of structures with abrupt stiffness degradations," *Mechanical Systems and Signal Processing*, vol. 163, Article ID 108131, 2022.
[22] C. C. Chang, J. F. Wang, and C. C. Lin, "An algorithm for parameter identifications of active mass damper and primary systems based on acceleration measurements," in *Proceedings of the ASME Pressure Vessels and Piping Conference*, vol. 58035, Waikoloa, HI, USA, October 2017.
[23] J. F. Wang and C. C. Lin, "Extracting parameters of TMD and primary structure from the combined system responses," *Smart Structures and Systems*, vol. 16, no. 5, pp. 937–960, 2015.
[24] N. Kang, H. Kim, S. Y. Choi, J. Hwang, and E. Yu, "Performance evaluation of TMD under typhoon using system identification and inverse wind load estimation," *Computer-Aided Civil and Infrastructure Engineering*, vol. 27, no. 6, pp. 455–473, 2012.
[25] L. J. Liu, Y. Su, J. Zhu, and Y. Lei, "Data fusion based EKF-UI for real-time simultaneous identification of structural systems and unknown external inputs," *Measurement*, vol. 88, pp. 456–467, 2016.
[26] J. N. Yang, A. K. Agrawal, B. Samali, and J. C. Wu, "Benchmark problem for response control of wind-excited tall buildings," *Journal of Engineering Mechanics*, vol. 130, no. 4, pp. 437–446, 2004.